

# The *in vitro* antiviral activity of lactoferrin against common human coronaviruses and SARS-CoV-2 is mediated by targeting the heparan sulfate co-receptor

Yanmei Hu<sup>a</sup>, Xiangzhi Meng<sup>b</sup>, Fushun Zhang<sup>b</sup>, Yan Xiang<sup>b</sup> and Jun Wang<sup>id</sup><sup>a</sup>

<sup>a</sup>Department of Pharmacology and Toxicology, College of Pharmacy, The University of Arizona, Tucson, AZ, USA; <sup>b</sup>Department of Microbiology, Immunology and Molecular Genetics, University of Texas Health Science Center at San Antonio, San Antonio, TX, USA

## ABSTRACT

Coronavirus disease 2019 (COVID-19) is an ongoing pandemic that lacks effective therapeutic interventions. SARS-CoV-2 infects ACE2-expressing cells and gains cell entry through either direct plasma membrane fusion or endocytosis. Recent studies have shown that in addition to ACE2, heparan sulfate proteoglycans (HSPGs) also play an important role in SARS-CoV-2 cell attachment by serving as an attachment factor. Binding of viral spike protein to HSPGs leads to the enrichment of local concentration for the subsequent specific binding with ACE2. We therefore hypothesize that blocking the interactions between viral spike protein and the HSPGs will lead to inhibition of viral replication. In this study, we report our findings of the broad-spectrum antiviral activity and the mechanism of action of lactoferrin (LF) against multiple common human coronaviruses as well as SARS-CoV-2. Our study has shown that LF has broad-spectrum antiviral activity against SARS-CoV-2, HCoV-OC43, HCoV-NL63, and HCoV-229E in cell culture, and bovine lactoferrin (BLF) is more potent than human lactoferrin. Mechanistic studies revealed that BLF binds to HSPGs, thereby blocking viral attachment to the host cell. The antiviral activity of BLF can be antagonized by the HSPG mimetic heparin. Combination therapy experiment showed that the antiviral activity of LF is synergistic with remdesivir in cell culture. Molecular modelling suggests that the N-terminal positively charged region in BLF (residues 17-41) confers the binding to HSPGs. Overall, LF appears to be a promising drug candidate for COVID-19 that warrants further investigation.

**ARTICLE HISTORY** Received 26 December 2020; Revised 29 January 2021; Accepted 5 February 2021

**KEYWORDS** SARS-CoV-2; COVID-19; lactoferrin; heparan sulfate; heparin

## Introduction

The coronavirus disease 2019 (COVID-19) has led to more than 100 million infections and over 2.1 million deaths worldwide, and more than 25 million infections and over 429,000 deaths in the US alone as of 28 January, 2021, rendering it one of the most life-threatening infectious disease outbreaks in human history. Severe acute respiratory syndrome coronavirus 2 (SARS-CoV-2), the causative agent of COVID-19 [1], together with severe acute respiratory syndrome coronavirus (SARS-CoV) [2], and Middle East respiratory syndrome coronavirus (MERS-CoV) [3], are the three highly pathogenic human coronaviruses that cause severe respiratory syndrome, while the other four common human coronaviruses (HCoV-229E, HCoV-NL63, HCoV-OC43 and HCoV-HKU1) account for 15–30% global cases of common cold in humans [4]. Limited number of therapeutics including vaccines and small molecules are available for COVID-19 treatment. As future coronavirus outbreak is highly possible, it is desired to develop broad-spectrum antivirals that are suitable for the prevention and

treatment of both current circulating CoVs and future emerging CoVs.

Lactoferrin (LF), a naturally occurring, non-toxic iron-binding glycoprotein present in several mucosal secretions, plays an important role in the first line of defence against microbial infections [5]. It is known that LF has broad-spectrum antiviral activity against a wide range of human and animal viruses including both DNA and RNA viruses [6,7]. Moreover, the anti-inflammatory and immunomodulatory activities of LF may have additional benefits in severe infections [8]. Furthermore, the presence of an intestinal receptor for the uptake of LF following oral administration [9], resistance to proteolytic degradation by trypsin and trypsin-like enzymes [10], and several established oral delivery systems for LF [11], ensures its oral bioavailability.

The reported antiviral mechanisms of LF include (1) direct binding to viral protein and inhibition of the adsorption of virus to the target cells [12–14]; (2) binding to heparan sulfate proteoglycans (HSPGs) on the host cell surface, which reduces viral

**CONTACT** Jun Wang  [junwang@pharmacy.arizona.edu](mailto:junwang@pharmacy.arizona.edu), [upennchainin@gmail.com](mailto:upennchainin@gmail.com)  Department of Pharmacology and Toxicology, College of Pharmacy, The University of Arizona, Tucson, AZ 85721, United States

© 2021 The Author(s). Published by Informa UK Limited, trading as Taylor & Francis Group, on behalf of Shanghai Shangyixun Cultural Communication Co., Ltd. This is an Open Access article distributed under the terms of the Creative Commons Attribution License (<http://creativecommons.org/licenses/by/4.0/>), which permits unrestricted use, distribution, and reproduction in any medium, provided the original work is properly cited.

attachment and subsequent viral entry [15–19]. Heparan sulfate (HS) is a linear and sulfated polysaccharide that is abundantly expressed on the surface of almost all cell types in the forms of HSPGs. The negatively charged HSPGs often serve as an attachment factor for a diverse of viruses [20,21]; (3) interfere with intracellular trafficking of virus [22]. LF was reported to have antiviral activity against SARS-CoV [17]. However, the broad-spectrum antiviral activity and antiviral mechanism of action of LF against common human coronaviruses as well as SARS-CoV-2 have not been systematically studied and therefore warrants further investigation. In this work, we profiled the broad-spectrum antiviral activity of LF against multiple common human coronaviruses including HCoV-OC43, HCoV-NL63, and HCoV-229E as well as SARS-CoV-2 and its mechanism of action. It was found that LF inhibits not only SARS-CoV-2, but also HCoV-OC43, HCoV-NL63, and HCoV-229E. The antiviral mechanism of action of LF was found to be mediated through binding to HSPGs on the host cell surface, thereby preventing viral attachment to the host cells. Several recent studies suggest that HSPGs serve as an attachment factor for the initial tethering of SARS-CoV-2 spike protein to host cell membrane and facilitates the subsequent binding to the specific receptor ACE2 [23–26]. Specifically, drug time-of-addition experiment and SARS-CoV-2 pseudovirus assays indicated that LF exerts its antiviral activity by blocking viral attachment to target cells. In addition, LF has direct binding to heparin, a mimetic of HSPGs, and pre-mixing LF with heparin decreased the inhibitory activity of LF on viral attachment and reduced antiviral activity of LF in cell culture. Furthermore, we have shown that LF has synergistic antiviral effect with remdesivir, which further warrants its development as a potential anti-coronavirus agent against both current circulating and future emerging coronaviruses.

## Results

### **Both bovine and human lactoferrins have broad-spectrum antiviral activity against multiple HCoVs in cell culture**

The antiviral activity of bovine and human lactoferrins was first tested in cytopathogenic effect (CPE) assay in cell culture against multiple HCoVs, including HCoV-229E, HCoV-NL63, and HCoV-OC43. Bovine lactoferrin (BLF) exhibited potent antiviral activity against all three HCoVs tested, with 50% effective concentration ( $EC_{50}$ ) values ranging from 11.2 to 37.9  $\mu\text{g}/\text{ml}$  (Figure 1(A,E)). Human lactoferrin (HLF) also showed potent antiviral activity against all three HCoVs tested, however, it was about 3–8 folds less potent than BLF with  $EC_{50}$  values ranging from 35.7

to 117.9  $\mu\text{g}/\text{ml}$  (Figure 1(B,E)). Both BLF and HLF were not cytotoxic to the cells at the concentration ranges tested (Figure 1(A–D), blue lines). Significantly, BLF also inhibited SARS-CoV-2 replication in Vero E6 cells with an  $EC_{50}$  value of  $571.5 \pm 72.8 \mu\text{g}/\text{ml}$  in the immunofluorescence imaging assay (Figure 1(A,E)). Given the higher inhibitory potency of BLF versus HLF, BLF was chosen for the following experiments. To confirm the antiviral activity of BLF, a secondary viral yield reduction (VYR) assay was performed to determine the effect of BLF treatment on infectious virus production. As measured in plaque assay, BLF dose-dependently inhibited infectious virion production of HCoV-229E, HCoV-NL63, and HCoV-OC43 in cell culture at 2 days post infection (dpi), with  $EC_{50}$  values ranging from 9.6 to 45.9  $\mu\text{g}/\text{ml}$  (Figure 1(C,E)). Next, to test the inhibitory effect of BLF on viral replication over time, HCoV-229E, HCoV-NL63, and HCoV-OC43 were amplified with and without BLF in MRC-5, Vero E6, and rhabdomyosarcoma (RD) cells, respectively, and the viral titers in the cell culture supernatants were quantified at different time points post-viral infection by plaque assay (Figure 1(D)). It was found that BLF decreased the viral titers of all three viruses by more than 2  $\log_{10}$  units at all time points, and it significantly inhibited the viral replication of HCoV-NL63, as there was no obvious viral titer increase up to 120 h post infection (hpi) (Figure 1(D), middle panel). Taken together, both BLF and HLF had potent antiviral activity against multiple common HCoVs and SARS-CoV-2, indicating LF is a promising antiviral drug candidate.

### **BLF inhibits infectious HCoV-OC43 and SARS-CoV-2 pseudovirus replication by blocking viral attachment to the host cell**

To elucidate the antiviral mechanism of action of BLF, the drug time-of-addition experiments were carried out to determine at which step(s) of viral replication BLF exerts its antiviral activity (Figure 2(A–D)). For this, 1000  $\mu\text{g}/\text{ml}$  of BLF was added to the cell culture at different time points of viral replication (Figure 2(B)) including viral attachment and onwards (#1), viral attachment and entry (#2), viral attachment only (#3), viral entry and onwards (#4), viral entry only (#5), and different time points post-viral entry (#6–#9). For this mechanistic study, HCoV-OC43 was chosen as a representative example of common human coronaviruses, and SARS-CoV-2 pseudovirus was used as a surrogate for the infectious SARS-CoV-2. In the first set of time-of-addition experiment, RD cells were infected with HCoV-OC43 at an MOI of 1, and intracellular viral protein expression was quantified by immunofluorescence staining using HCoV-OC43 specific antibody (Figure 2(A)), and viral titers

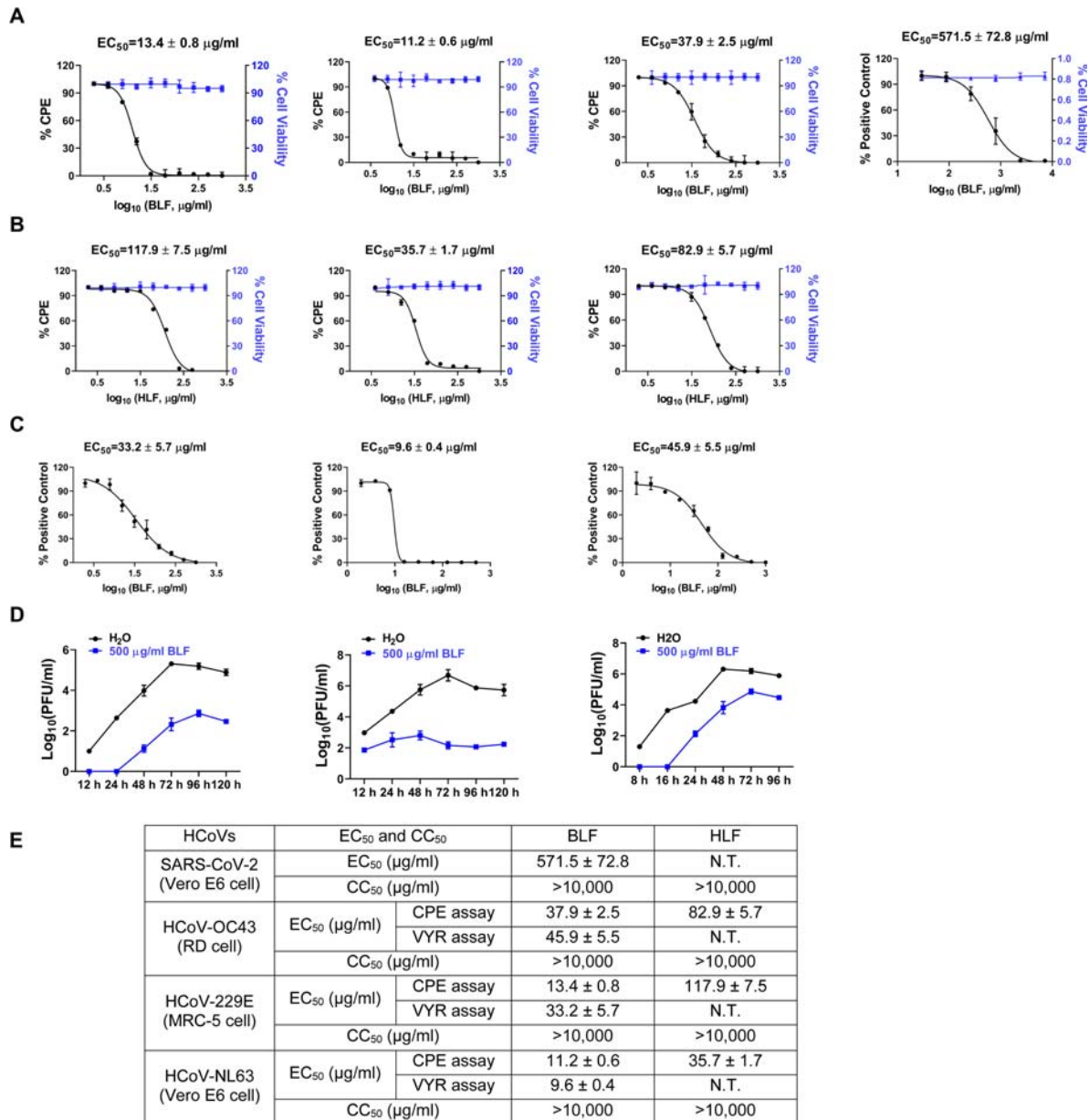


**Figure 1.** Antiviral activity of bovine and human lactoferrins against multiple common HCoVs and SARS-CoV-2 in cell culture. (A) The antiviral activity of bovine lactoferrin (BLF) against HCoV-229E, HCoV-NL63, HCoV-OC43 in CPE assay and SARS-CoV-2 in immunofluorescence imaging assay (from left to right). (B) The antiviral activity of human lactoferrin (HLF) against HCoV-229E, HCoV-NL63, HCoV-OC43 in CPE assay (from left to right). (C) Secondary viral yield reduction (VYR) assay of BLF against HCoV-229E, HCoV-NL63, HCoV-OC43 (from left to right). (D) Growth curves of HCoV-229E, HCoV-NL63, HCoV-OC43 (from left to right) in the absence (black) or presence of 500 µg/ml BLF (blue). EC<sub>50</sub> curve fittings in the CPE and VYR assays were obtained using log<sub>10</sub> (concentration of inhibitors) vs. percentage of CPE or percentage of positive control with variable slopes in prism 8. The cellular cytotoxicity test was included in CPE experiment and the resulting curves were shown in blue. All data are mean ± standard deviation of three replicates. (E) EC<sub>50</sub> and CC<sub>50</sub> values of BLF and HLF against multiple HCoVs and SARS-CoV-2 in cell culture.

of progeny virus released into the cell culture medium were quantified by plaque assay (Figure 2(C)). The immunofluorescence assay results showed that BLF only inhibited viral replication when it was included in the viral attachment stage (Figure 2(A), #1, #2, and #3), and it had no significant antiviral effect when added during the viral entry and post-viral entry (Figure 2(A), #4–#9). Consistent with the immunofluorescence assay results, viral titers were significantly decreased when BLF was present at steps including viral attachment (Figure 2(C), #1–#3), but

not in the entry and post-entry steps (Figure 2(C), #4–#8). To test whether BLF inhibits SARS-CoV-2 through a similar mechanism, SARS-CoV-2 pseudovirus particles were used in the second set of time-of-addition experiment. The relative titers of SARS-CoV-2 pseudoviral particles were determined by measuring the ratio of luciferase reporter gene expression level with and without LF treatment. The results demonstrated that BLF inhibited SARS-CoV-2 pseudovirus replication at the attachment stage (Figure 2(D), #1–#3), but not viral entry and post-

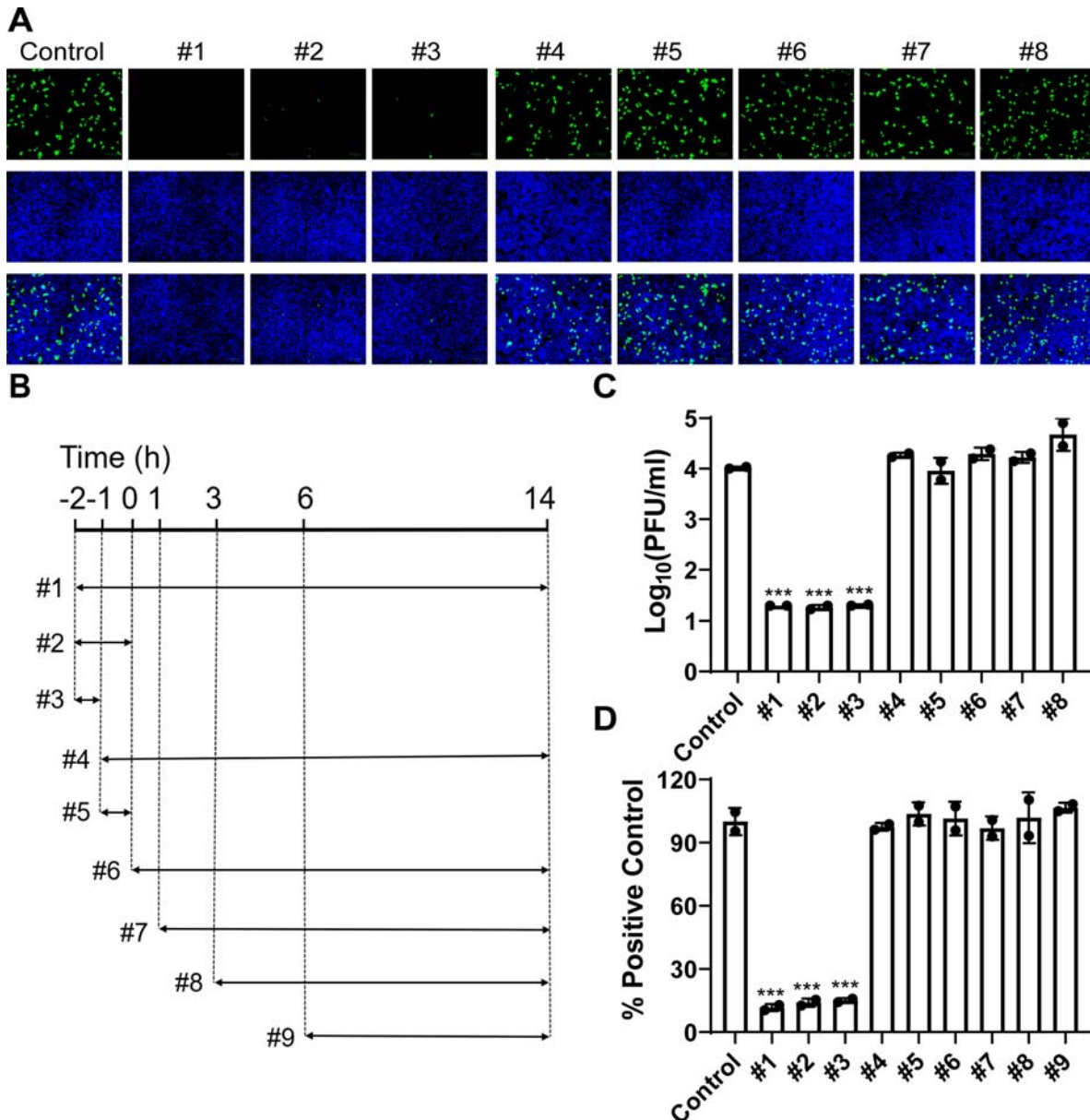


**Figure 2.** Time-of-addition experiments of BLF with HCoV-OC43 or SARS-CoV-2 pseudovirus particles. (A) Representative images of intracellular HCoV-OC43 virus detected by immunofluorescence staining using HCoV-OC43 specific antibody. Images were taken by Zoe™ Fluorescent Cell Imager (BioRad). (B) Illustration of the time periods when BLF (1000 µg/ml) was present in the time-of-addition experiments. Arrows represent the periods of time that BLF was present in the cell culture. (C) Quantification of HCoV-OC43 virus released into the cell culture medium using plaque assay. (D) Relative SARS-CoV-2 pseudovirus particle titers were quantified by measuring luciferase activity using Bright-Glo Luciferase Assay System and normalized to control. \*\*\*,  $p < 0.001$  (student's *t*-test). Data are mean  $\pm$  standard deviation of two replicates.

entry stages (Figure 2(D), #4–#9). Collectively, the drug time-of-addition results suggested that LF blocks viral attachment to host cells and has no effect on viral replication when added post-viral entry.

#### LF inhibits SARS-CoV-2 pseudovirus replication in multiple cell lines

Pseudovirus neutralization assay is an established model to study the mechanism of viral entry into host cells and has been widely used to assess the antiviral activity of viral entry/fusion inhibitors [27–29]. To test whether the antiviral effect of lactoferrins against SARS-CoV-2 is cell type dependent, BLF and

HLF were tested in SARS-CoV-2 pseudovirus assay in three different types of cell lines: Vero E6 cell (Figure 3(A)), Calu-3 cell (Figure 3(B)), and 293T cell overexpressing ACE2 (293T-ACE2) (Figure 3(C)). Vero E6 and 293T-ACE2 cells express high levels of ACE2 on the apical membrane domain but minimal levels of transmembrane serine proteinase 2 (TMPRSS2), the host serine protease that cleaves viral spike protein [30]. As such, SARS-CoV-2 virus enters these cells through endocytosis and relies on endosomal cathepsin L for viral spike protein activation [31,32]. In contrast, Calu-3 is a human lung epithelial cell line with endogenous expression of both ACE2 and TMPRSS2 [33], and SARS-CoV-2

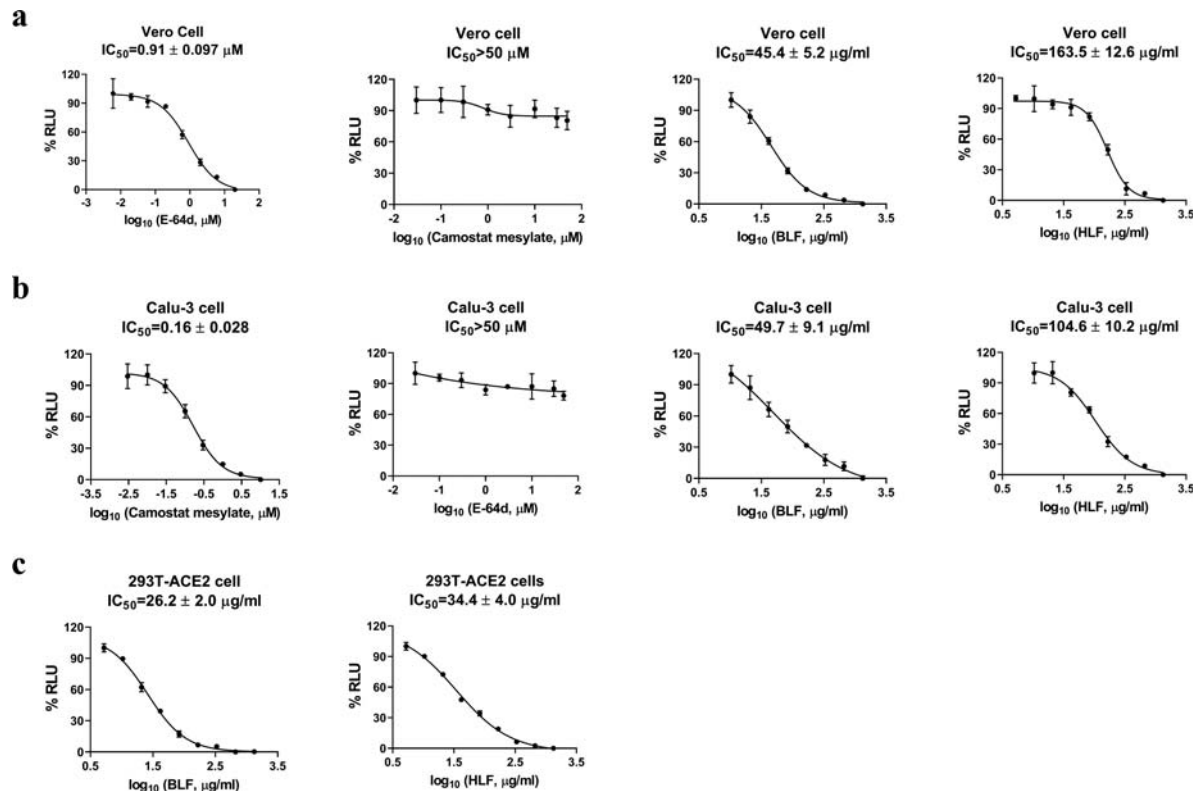


**Figure 3.** Inhibitory activity of BLF and HLF in the SARS-CoV-2 pseudovirus neutralization assay in different cell lines. (A) Vero E6 cell. (B) Calu-3 cell. (C) 293T cell overexpressing ACE2. Cathepsin L inhibitor E-64d and TMPRSS2 inhibitor camostat mesylate were included as controls in Vero E6 and Calu-3 cells, respectively.  $IC_{50}$  curve fittings using  $\log_{10}$  (concentration of inhibitors) vs. percentage of DMSO control with variable slopes were performed in Prism 8. All data are mean  $\pm$  standard deviation of two replicates.

spike protein can be activated at the cell surface by TMPRSS2, resulting in direct cell entry at the plasma cell membrane. Previously reported cathepsin L inhibitor E-64d and TMPRSS2 inhibitor camostat mesylate were included as controls for the SARS-CoV-2 pseudovirus entry assays. It was found that both BLF and HLF inhibited SARS-CoV-2 pseudovirus entry in a dose-dependent manner in all three cell lines, with  $IC_{50}$  values ranging from 26.2 to 49.7  $\mu\text{g/ml}$  and 34.4–163.5  $\mu\text{g/ml}$ , respectively (Figure 3). BLF was more potent than HLF, which agrees with the antiviral assay results from the infectious HCoV-229E (Figure 1). These results indicate that the inhibition of SARS-CoV-2 pseudovirus entry by lactoferrins is cell type independent.

#### **LF blocks viral attachment through interaction with the host cell instead of the virus**

SARS-CoV-2 attaches to the host cells through the interactions between viral spike protein and host cell ACE2 receptor and HSPGs attachment factor [23]. To determine whether LF interferes with viral attachment through interacting with the host cell or the virus, we used the HCoV-OC43 virus or the SARS-CoV-2 pseudovirus particles as SARS-CoV-2 surrogates and performed cell pretreatment and virucidal experiments. The results demonstrated that

pretreatment of RD cells with 1000  $\mu\text{g/ml}$  BLF prior to viral infection reduced intracellular viral protein expression level by about 80% compared to the  $\text{H}_2\text{O}$ -treated control sample (Figure 4(A,B)), and the viral titer in the supernatant was decreased by about 1  $\log_{10}$  unit in the presence of 1000  $\mu\text{g/ml}$  BLF (Figure 4(C)). Similarly, pretreatment of Vero E6 cells with 1000  $\mu\text{g/ml}$  BLF decreased the SARS-CoV-2 pseudovirus luciferase activity to about 50% of the  $\text{H}_2\text{O}$ -treated control (Figure 4(D)). To assess the direct effect of LF on HCoV-OC43 viral particles, HCoV-OC43 viruses were pre-treated with 1000  $\mu\text{g/ml}$  BLF or same volume of sterile  $\text{H}_2\text{O}$  (untreated control) at 37 °C for 3 h, followed by viral titer quantification by plaque assay in RD cells. It was found that BLF-treated virus showed the same number of plaques as the  $\text{H}_2\text{O}$ -treated control at  $10^{-6}$ -fold dilution (Figure 4(E)). The final concentration of BLF in the plaque assay was 0.001  $\mu\text{g/ml}$ , far below its minimum inhibitory concentration ( $EC_{50} = 37.9 \pm 2.5 \mu\text{g/ml}$ ) and thus had no effect on plaque formation. Taken together, these results suggested that BLF inhibits viral attachment through binding to host cells instead of the virus.

#### **BLF and HLF bind to heparin in vitro**

Previous study reported that LF blocks SARS-CoV pseudovirus infection in HEK293E/ACE2-Myc cells

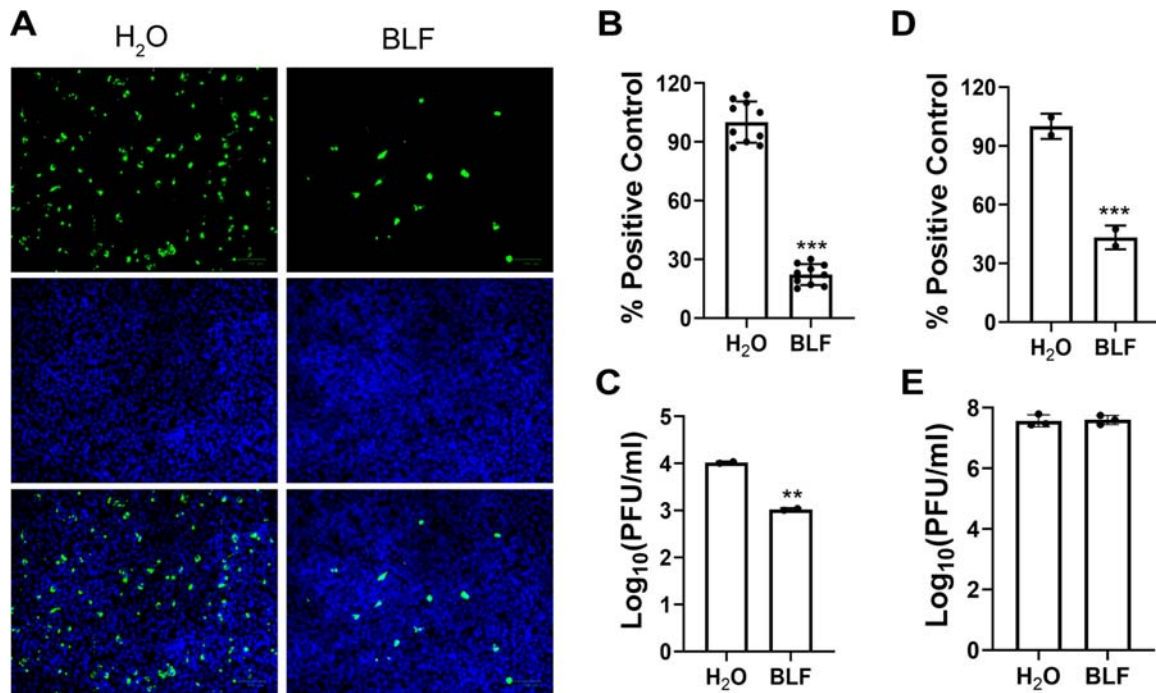
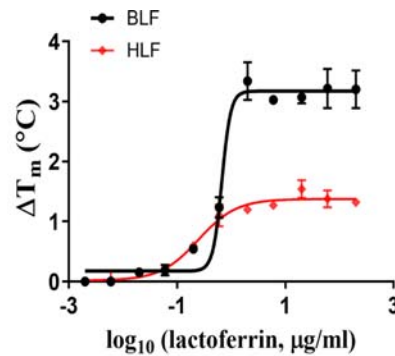


**Figure 4.** Evaluation of the direct effect of BLF on host cells or viral particles through pretreatment of cells or virus. (A) Representative immunofluorescence images of pretreating cells with 1000  $\mu\text{g/ml}$  BLF or H<sub>2</sub>O. (B) Quantification of the results from panel (A). (C) Viral titers of HCoV-OC43 from cell culture medium of RD cells pre-treated with H<sub>2</sub>O or 1000  $\mu\text{g/ml}$  BLF. (D) Expression levels of luciferase reporter gene in SARS-CoV-2 pseudovirus particles infected Vero E6 cells pre-treated with H<sub>2</sub>O or 1000  $\mu\text{g/ml}$  BLF. (E) Infectious viral titers of HCoV-OC43 virus pre-treated with 1000  $\mu\text{g/ml}$  BLF or H<sub>2</sub>O. \*\*,  $p < 0.01$ ; \*\*\*,  $p < 0.001$  (student's  $t$ -test). Data are mean  $\pm$  standard deviation of three replicates.

by binding to HSPGs on the cell surface [17]. In addition, HCoV-NL63 was shown to utilize HSPGs as adhesion receptor for viral attachment to target cells through its interaction with the membrane (M) protein [18,19]. Recently, cell surface HSPGs were discovered as the co-receptors for SARS-CoV-2 spike (S) protein and facilitate the subsequent binding to ACE2 receptor [23,24,26]. Based on these findings and our results listed above, we hypothesize that LF exerts its broad-spectrum antiviral activity against coronaviruses by binding to HSPGs, therefore indirectly blocking the interaction between viral spike protein and ACE2. To test this hypothesis, we chose heparin (Sigma Cat.# H3393) as a mimetic of HSPGs, and performed the differential scanning fluorimetry (DSF) assay [34] to determine the direct binding of heparin to BLF and HLF. Specific binding of a ligand to a protein typically stabilizes the target protein, resulting in an increased melting temperature ( $T_m$ ). DSF results demonstrated that heparin increased the  $T_m$  of both BLF and HLF in a dose-dependent manner (Figure 5), indicating the direct binding of BLF and HLF to heparin. In addition, BLF displayed higher binding affinity than HLF to heparin as shown by the larger  $\Delta T_m$ , and this result agrees with the more potent antiviral activity of BLF compared to HLF.

Next, to confirm that BLF blocks viral attachment to target cells, a viral attachment assay was carried out in the presence of different combinations of LF

and/or heparin, and the attached HCoV-OC43 or HCoV-NL63 on the surface of RD cells or Vero E6 cells were quantified by immunofluorescence staining (Figure 6(A)) and real-time PCR (Figure 6(B,C)). Fluorescent signals were detected on the surface of RD cells that were treated with H<sub>2</sub>O control (Figure 6(A), #1), indicating the binding of HCoV-OC43 virus to the host cell surface. BLF-treated samples showed dose-dependent decrease of fluorescent signals on the cell surface (Figure 6(A), #2–#3), suggesting BLF inhibited viral attachment. Heparin treatment alone had no significant effect on viral attachment (Figure 6(A), #4–#5) as shown by the immunofluorescence intensity. In contrast, pretreatment of BLF with heparin before adding the mixture to the viral attachment assay abolished the inhibition of viral attachment as the fluorescence signals were restored (19% at 10  $\mu\text{g/ml}$  and 86% at 30  $\mu\text{g/ml}$  of heparin) (Figure 6(A), #6–#7). No specific antibody against HCoV-NL63 was available, so the immunofluorescence assay was not performed for HCoV-NL63. Instead, we quantified the amount of cell surface-attached viruses by RT-qPCR. Both HCoV-OC43 and HCoV-NL63 viral RNA levels were significantly reduced in a dose-dependent manner with BLF treatment alone: ~15% and ~5% of HCoV-OC43 viral RNA were detected with 500 and 1000  $\mu\text{g/ml}$  BLF treatment; ~0.5% and ~0% of HCoV-NL63 viral RNA were detected with 500 and 1000  $\mu\text{g/ml}$  BLF



heparin Conc. (µg/ml)	BLF		HLF	
	$T_m$ (°C)	$\Delta T_m$ (°C)	$T_m$ (°C)	$\Delta T_m$ (°C)
0	85.65 ± 0.49		66.39 ± 0.26	
0.02	85.81 ± 0.47	0.50	66.26 ± 0.29	-0.13
0.06	85.74 ± 0.76	0.44	66.68 ± 0.47	0.29
0.2	86.20 ± 0.52	0.89	66.58 ± 0.32	0.19
0.6	86.89 ± 0.73	1.58	67.04 ± 0.03	0.65
2	88.99 ± 0.48	3.69	67.28 ± 0.68	1.08
6	88.63 ± 0.37	3.32	67.63 ± 0.02	1.24
20	88.57 ± 0.57	3.27	67.65 ± 0.59	1.26
60	88.87 ± 0.03	3.56	67.78 ± 0.05	1.39
200	88.85 ± 0.04	3.55	67.63 ± 0.03	1.24

**Figure 5.** Effect of heparin on melting temperature ( $T_m$ ) of BLF and HLF. Data were plotted with  $\Delta T_m$  vs.  $\log_{10}$  (concentrations of heparin) using Boltzmann Sigmoidal equation in Prism 8 (left).  $T_m$  of lactoferrins in the absence or presence of indicated concentrations of heparin are shown in the table, and  $\Delta T_m$ s were calculated by subtracting the  $T_m$  of LF without heparin. Data are mean  $\pm$  standard deviation of two replicates.

treatment (Figure 6(B,C)). Heparin itself had no obvious effect on viral RNA levels at the indicated concentrations (10 and 30 µg/ml) (Figure 6(B,C)). However, BLF lost partial potency in the presence of 10 or 30 µg/ml heparin: ~45% or ~75% of HCoV-OC43 viral RNA and ~25% or 60% HCoV-NL63 viral RNA were detected under these conditions (Figure 6(B,C)). Collectively, the results suggest that BLF interferes viral attachment through its interaction with cell surface HSPGs.

#### Heparin decreases antiviral activity of BLF in cell culture

As illustrated above, BLF was shown to block viral attachment to the host cells and this inhibitory effect was neutralized by pre-mixing with heparin, therefore, it is expected that the cellular antiviral activity of BLF will decrease in the presence of heparin. To this end, the antiviral potency of BLF against HCoV-229E, HCoV-NL63 and HCoV-OC43 were determined in the absence or presence of different concentrations of heparin (Figure 7(A–C)). We first determined the antiviral activity of heparin from two different sources (Cat.# H3393 and Cat.# H3149) in CPE assay in cell cultures. Both heparins had  $EC_{50}$  values of a few hundred micromoles against all three HCoVs tested (Figure 7(D)), which is consistent with previous reported results [35]. To avoid the interference of

antiviral activity from heparin, four concentrations of heparin (1, 3, 10 and 30 µg/ml), which are far below its minimum inhibitory concentration, were chosen to determine the effect of heparin on the antiviral potency of BLF in the CPE assay. Heparin decreased the antiviral activity of BLF against all three HCoVs tested in a dose-dependent manner (Figure 7(A–C)), with the  $EC_{50}$  values of BLF increased from 2 to >100-folds in the presence of heparin (Figure 7(D)).

#### BLF has synergistic antiviral effect with remdesivir in cell culture

Combination therapy has been extensively explored for the treatment in oncology, parasitic, bacterial and viral infections [36–38], it has many advantages over monotherapies such as delayed development of drug resistance; synergistic efficacy on treatment; and fewer side effects due to the lower doses of drugs used. The combination treatment potential of BLF with remdesivir was explored using HCoV-OC43 antiviral CPE assay. Remdesivir is a SARS-CoV-2 polymerase inhibitor and is an FDA-approved antiviral. Combination indices (CIs) versus the  $EC_{50}$  values of compounds at different combination ratios were plotted as previously described [39]. The red line indicates additive effect; the right upper area above the red line indicates antagonism, while the

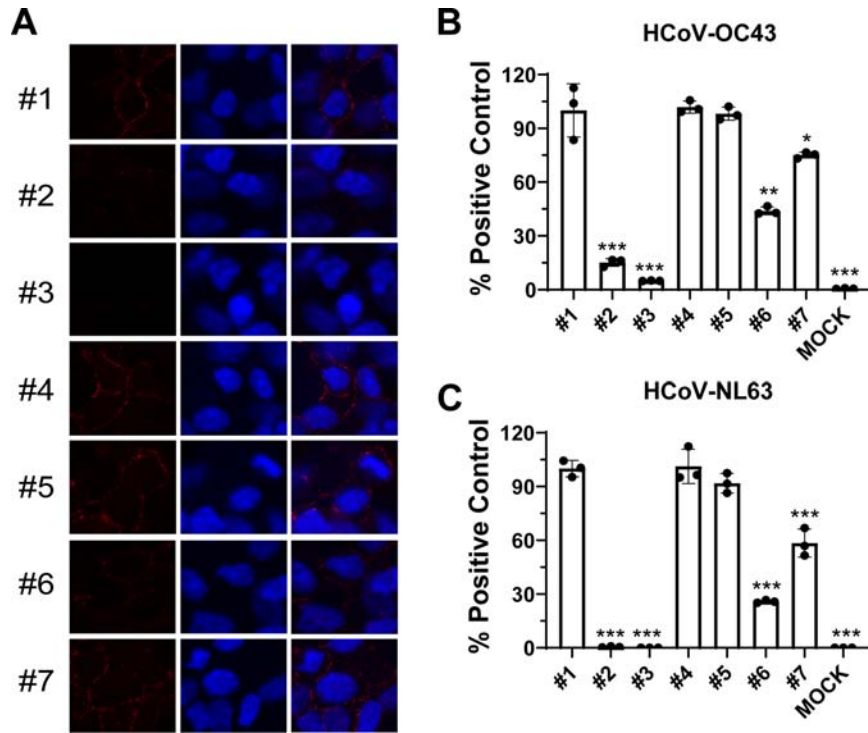


**Figure 6.** Heparin reduced the inhibitory activity of BLF on viral attachment to target cells. (A) Representative immunofluorescence images of HCoV-OC43 attached to RD cell surface detected by immunofluorescence staining. (B) Quantification of HCoV-OC43 attached to RD cell surface detected by RT-qPCR of N gene. (C) Quantification of HCoV-NL63 attached to Vero E6 cell surface detected by RT-qPCR of N gene. #1: H<sub>2</sub>O; #2: 500 µg/ml BLF; #3: 1000 µg/ml BLF; #4: 10 µg/ml heparin; #5: 30 µg/ml heparin; #6: 500 µg/ml BLF+10 µg/ml heparin; #7: 500 µg/ml BLF+30 µg/ml heparin. \*,  $p < 0.05$ ; \*\*,  $p < 0.01$ ; \*\*\*,  $p < 0.001$  (student's *t*-test). All data are mean  $\pm$  standard deviation of three replicates.

left bottom area below the line indicates synergy [39]. In all combination scenarios, the CIs at all the combination ratios fell below the red line (Figure 7(E)), suggesting BLF displayed synergistic antiviral effect with remdesivir in the combination therapy.

### Modelling the binding between BLF and HSPGs

LF is a single chain 80-kDa iron-binding glycoprotein that belongs to the transferrin family. It contains two symmetric N- and C-globular lobes. Multiple studies have shown that the heparin-binding site of BLF is located at the N-terminal domain of the N-lobe, which contains a cluster of positive charges spanning residues 17–41 [40]. This positively charged domain confers to the antiviral activity against adenovirus [41], papillomavirus [42], and echovirus 6 [43]. The trypsin digested N-terminal peptide lactoferricin alone is sufficient to prevent adenovirus, herpes simplex virus (HSV), and cytomegalovirus (CMV) infection [41,44,45]. It was found that the N-terminal domain of BLF is more negatively charged than HLF (Figure 8(A) vs. 8(B), and 8(C)), which might explain the more potent antiviral activity of BLF than HLF in inhibiting human papillomavirus, HSV, and HCMV [42,44,45]. Our data similarly showed that BLF is more potent than HLF in inhibiting common human coronaviruses including HCoV-OC43, HCoV-229E,

and HCoV-NL63 (Figure 1(A) vs. 1(B)). To gain insights how BLF binds to HSPGs, we chose the bovine lactoferricin (PDB: 1LFC) [46] and dp4 (PDB: 5E9C) [47] as structural models of BLF and HSPGs, respectively. Docking model showed that the negatively charged sulfate in dp4 engages multiple electrostatic interactions with the positive charges from Arg25, Lys27, and Arg39 (Figure 8(D,E)).

Collectively, the proposed antiviral mechanism of action of LF against coronaviruses is shown in Figure 8(F). SARS-CoV-2 viral particles are recruited to cell surface by interaction with HSPGs, facilitating subsequent specific binding to ACE2 receptor and following internalization of the virion. LF binds to cell surface HSPGs, which blocks the interaction between SARS-CoV-2 and HSPGs and subsequent viral attachment to host cells.

### Discussion

Several studies have shown that HSPGs are co-receptors for the SARS-CoV-2 infection [48]. Due to their negative charges, HSPGs help to recruit SARS-CoV-2 to the cell surface by interacting with the viral spike protein, thereby increasing the local concentration of the viral spike protein for more effective subsequent binding with ACE2. A recent computational model suggested that a positively charged

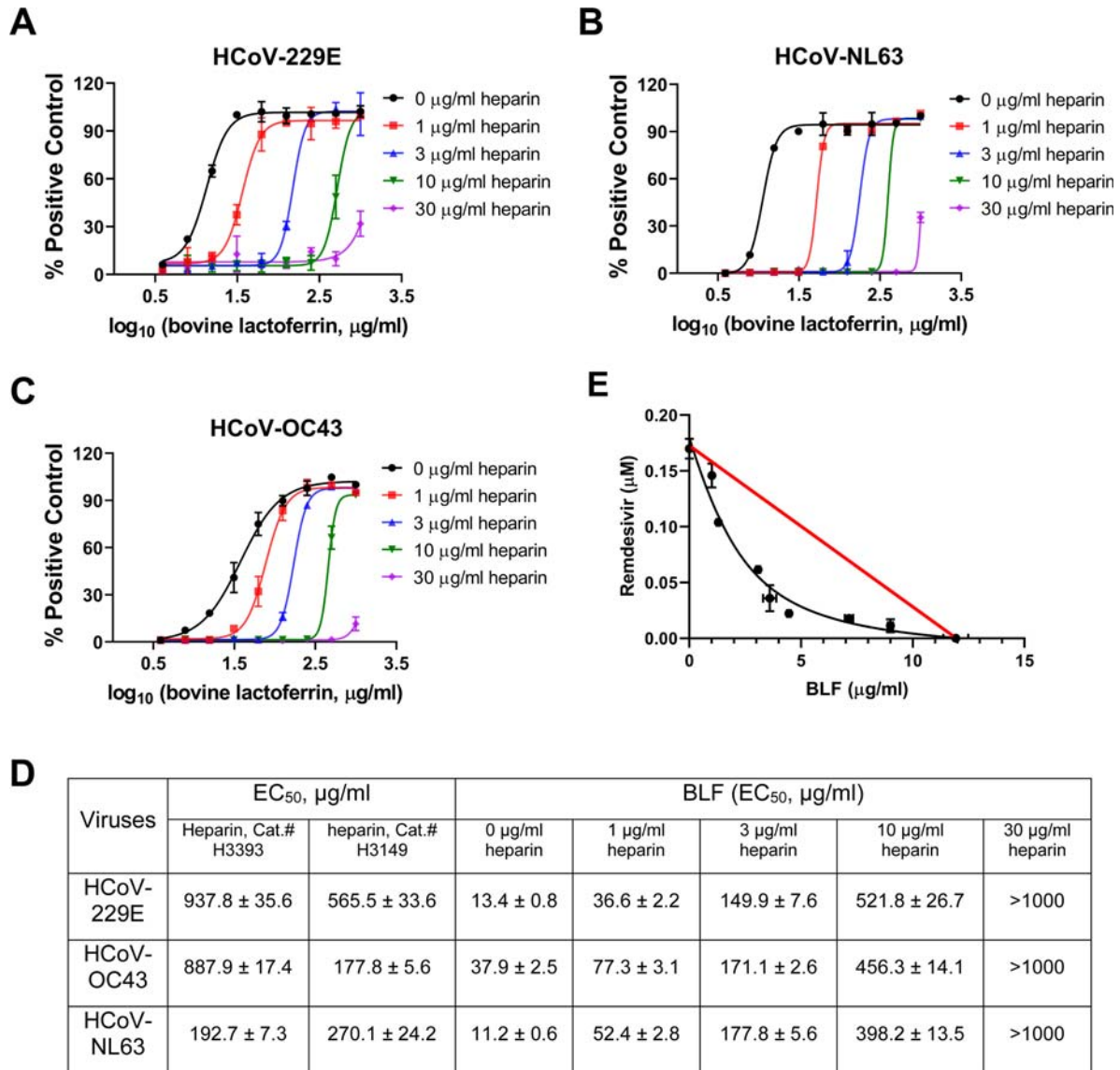


**Figure 7.** Antiviral potency of BLF in the absence or presence of different concentrations of heparin against HCoVs. Cells at near confluency were infected with (A) HCoV-229E; (B) HCoV-NL63; or (C) HCoV-OC43, different concentrations of BLF and indicated concentrations of heparin were mixed and immediately added into the cells for EC<sub>50</sub> determination. EC<sub>50</sub> curve fittings were obtained using log<sub>10</sub> (concentration of inhibitors) vs. percentage of positive control (uninfected cells) with variable slopes in prism 8. (D) Antiviral EC<sub>50</sub> values of BLF in the presence of different concentrations of heparin. (E) Combination therapy of remdesivir with BLF. Data are mean ± standard deviation of three replicates.

binding groove located at the viral spike protein RBD might be the putative binding site for the negatively charged HSPGs [23,24]. Binding study using surface plasma resonance assay showed that the monomer and trimer forms of SARS-CoV-2 spike glycoprotein bind to heparin with  $K_d$  values of  $4.0 \times 10^{-11}$  and  $7.3 \times 10^{-11}$  M, respectively [24]. In addition to SARS-CoV-2, SARS-CoV similarly relies on HSPGs as an anchor for viral attachment [17]. Likewise, HCoV-NL63 is also known to utilize its membrane protein to bind to HSPGs and facilitate tethering of virions to the host cell surface [18,19,49]. A drug repurposing screening identified several compounds targeting HSPGs and HSPGs-dependent endocytosis pathways as potent entry inhibitors for SARS-CoV and SARS-CoV-2 [26]. Given the importance of

HSPGs in coronavirus cell entry, it is plausible that compounds interfering with the binding between virus and HSPGs might inhibit viral replication. In this context, the endogenous natural protein LF becomes a prominent candidate due to its strong binding with HSPGs. Indeed, LF was previously shown to inhibit the SARS-CoV pseudovirus infection by blocking its interaction with HSPGs [17]. However, the antiviral activity of LF against infectious coronaviruses including SARS-CoV-2, HCoV-OC43, HCoV-NL63, and HCoV-229E has not been reported. Nevertheless, these results collectively suggest that HSPGs are a promising antiviral drug target for broad-spectrum antivirals against coronaviruses. In this study, we investigated the antiviral activity and mechanism of action of lactoferrins (BLF and HLF) against multiple

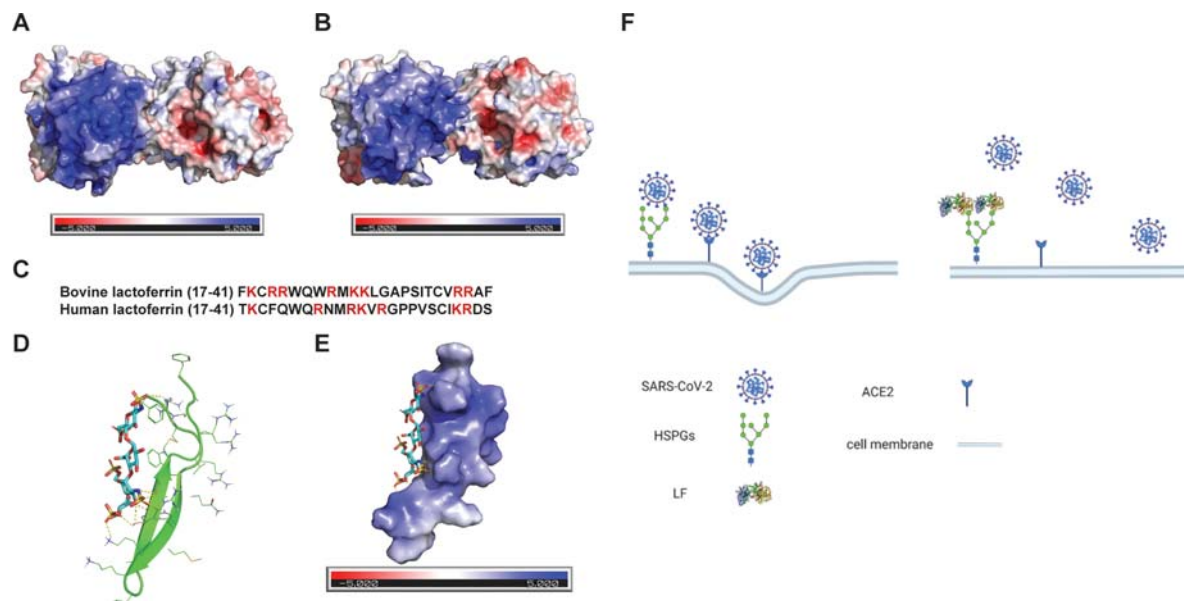


**Figure 8.** Structures of BLF, HLF, and the docking model of heparin dp4 with bovine lactoferrin. (A) Surface electrostatics of BLF (PDB: 1BLF). (B) Surface electrostatics of HLF (PDB: 1LFI). (C) Sequence alignment of the positively charged N-terminal domain of BLF and HLF. (D) Docking model of heparin dp4 with bovine lactoferrin (PDB: 1LFC). The heparin dp4 structure was from PDB 5E9C. (E) Surface view of the docking model of heparin dp4 with bovine lactoferrin. Docking was performed using AutoDock Vina and figures were generated using PyMOL. (F) Proposed antiviral mechanism of LF. The figure was created with BioRender.com.

coronaviruses. New findings and highlights of our study include: (1) BLF and HLF have broad-spectrum antiviral activity against infectious SARS-CoV-2, HCoV-OC43, HCoV-NL63, and HCoV-229E viruses in cell culture. It is noted that in parallel to our study, two preprints in biorxiv independently confirmed the antiviral activity of LF against SARS-CoV-2 [50,51]. (2) The inhibition of SARS-CoV-2 pseudovirus replication by BLF is not cell dependent, suggesting BLF might offer protection against SARS-CoV-2 infection in multiple tissues and organs. (3) The antiviral mechanism of action of BLF is through binding to host cell surface HSPGs (Figure 8(F)). Using SARS-CoV-2 pseudovirus and HCoV-OC43 as representative examples, we have shown that BLF inhibits viral attachment to the host cell and has no effect on viral entry and subsequent replication processes. The antiviral activity of BLF is diminished dose-dependently by exogenously added heparin. (4) BLF has synergistic antiviral effect with the FDA-approved SARS-CoV-2 antiviral remdesivir in cell culture. Collectively, this study provided compelling evidence to support the translational potential of LF as broad-spectrum antivirals for coronaviruses including SARS-CoV-2.

## Materials and methods

### Cell lines, viruses and reagents

Human RD, Vero E6 cell, Huh-7 cell, HEK293T cell expressing ACE2 (293T-ACE2), and HCT-8 cell lines were maintained in Dulbecco's modified Eagle's

medium (DMEM); Caco-2 cell, Calu-3 cell and MRC-5 cell lines were maintained in Eagle's Minimum Essential Medium (EMEM). Both mediums were supplemented with 10% fetal bovine serum (FBS) and 1% penicillin–streptomycin antibiotics. Cells were kept at 37 °C incubator in a 5% CO<sub>2</sub> atmosphere. The following reagent was obtained through BEI Resources, NIAID, NIH: Human Coronavirus, OC43, NR-52725 and was propagated on HCT-8 cell or RD cell; HCoV-229E was obtained from Dr. Bart Tarbet (Utah State University) and amplified on Huh-7 cell or MRC-5 cell; The following reagent was obtained through BEI Resources, NIAID, NIH: Human Coronavirus, NL63, NR-470 and propagated on Caco-2 cell or HEK293T cell expressing ACE2 cell (293T-ACE2).

BLF (Cat.# L9507), HLF (Cat.# L4894) and heparin sodium salt from porcine intestinal mucosa (Cat.# H3149 and Cat.# H3393) were purchased from Millipore Sigma (St. Louis, MO). LF were dissolved in sterile Nanopure water or PBS buffer with stock concentration of 10 mg/ml, heparin was dissolved in sterile Nanopure water with stock concentration of 50 mg/ml. Remdesivir was purchased from MedChemExpress and dissolved in DMSO before use.

### Antiviral assays

Antiviral activities of BLF or HLF against 229E, NL63 and OC43 were tested in CPE assays as previously described [52] with minor modifications. Briefly, cell cultures at near confluency in 96-well plates were infected with 100 µL of viruses at desired dilutions

and incubated for 1 h. Unabsorbed virus was removed and different concentrations of LF (0, 3.9, 7.8, 15.6, 31.3, 62.5, 125, 250, 500, 1000 µg/ml) were added. Remdesivir was included as a positive control. The plates were incubated for another 3–5 days when a significant cytopathic effect was observed in the wells without compound (virus only). Cells were stained with 0.1 mg/ml neutral red for 2 h, and excess dye was rinsed from the cells with PBS. The absorbed dye was eluted from the cells with buffer containing 50% ethanol and 1% glacial acetic acid. Plates were read for optical density determination at 540 nm. Readings were normalized with uninfected controls. EC<sub>50</sub> values were determined by plotting percent CPE versus log<sub>10</sub> compound concentrations from best-fit dose response curves with variable slope in Prism 8. Toxicity of LF at each concentration was determined in uninfected cells in the same microplates by measuring neutral red dye uptake.

VYR assays were conducted as previously described [53] with minor modifications. Viruses were first replicated in the presence of different concentrations of BLF. Supernatant was harvested 2 dpi from each concentration of test compound and the viral yield was determined by plaque reduction assay. The EC<sub>50</sub> values were calculated from best-fit dose response curves with variable slope in Prism 8.

Viral growth curves were obtained by replicating viruses in the presence or absence of BLF at MOI of 0.1. Viruses in the supernatant were collected at the indicated time-point post infection and viral titers were determined by plaque reduction assay. For all antiviral assays, LF was included during virus infection and post-infection stages.

### Time of addition

Drug time-of-addition experiment was performed as previously described [54,55]. Briefly, RD cells were seeded at  $1 \times 10^5$  cells/well in 12-well plate. 1000 µg/ml BLF was added at different time points of viral life cycle, as illustrated in Figure 2(B): –2 to –1 h (viral attachment), –1 to 0 h (viral entry), 0, 3, 6 to 14 h (post-viral entry). RD cells were infected with HCoV-OC43 at an MOI of 0.1 24 h after seeding. Viruses were harvested at 12 hpi. The viral titers were determined by plaque assay.

### Immunofluorescence imaging

HCoV-OC43 immunofluorescence staining was performed similarly as previously described [56] with minor modifications. For drug time-of-addition experiment using immunofluorescence staining, RD cells were infected with HCoV-OC43 at an MOI of 1. Viral infection started at the –2 h time-point and incubated at 4 °C for 1 h to allow virus attachment.

At –1 h time-point, unbound virus was removed and cells were washed with ice-cold PBS buffer. Same volume of medium without virus was added into each well and cells were incubated at 33 °C for 1 h to allow virus entry. At 14 h post infection (hpi), cells were fixed with 4% formaldehyde for 10 min followed by permeabilization with 0.2% Triton X-100 for another 10 min. After blocking with 5% bovine serum, cells were sequentially stained with anti-Coronavirus antibody, HCoV-OC43 strain, clone 541-8F (Cat#: MAB9012, Millipore Sigma, Burlington, Massachusetts, USA) as primary antibody, and anti-mouse secondary antibody conjugated to Alexa-488 or Alexa-546 (Cat # A-11029, Cat # A-11030, Thermo Scientific, Waltham, Massachusetts, USA). Nuclei were stained with 300 nM DAPI (Cat#: D1306, Thermo Scientific, Waltham, Massachusetts, USA) after secondary antibody incubation.

### Pseudovirus assay

A pseudotype HIV-1-derived lentiviral particles bearing SARS-CoV-2 Spike and a lentiviral backbone plasmid encoding luciferase as reporter was produced in HEK293T cells engineered to express the SARS-CoV-2 receptor, ACE2 (ACE2/293T cells), as previously described [27]. The pseudovirus was then used to infect Vero E6 cells or Calu-3 cells or ACE2/293T cells in 96-well plates in the presence of H<sub>2</sub>O or serial concentrations of E-64d, Camostat Mesylate or BLF or HLF. 48 hpi, cells from each well were lysed using the Bright-Glo Luciferase Assay System (Cat#: E2610, Promega, Madison, WI, USA), and the cell lysates were transferred to 96-well Costar flat-bottom luminometer plates. The relative luciferase units (RLUs) in each well were detected using Cytation 5 Cell Imaging Multi-Mode Reader (BioTek, Winooski, VT, USA).

### Differential scanning fluorimetry (DSF)

The binding of heparin and BLF was monitored by DSF using a Thermal Fisher QuantStudio™ 5 Real-Time PCR System as previously described [57] with minor modifications. TSA plates were prepared by mixing BLF (final concentration of 100 µg/ml) with different concentrations (0.02–200 µg/ml) of heparin and incubated at 30 °C for 1 h.  $1 \times$  SYPRO orange (Thermal Fisher) were added and the fluorescence of the plates were taken under a temperature gradient ranging from 20 to 95 °C (incremental steps of 0.05 °C/s). The melting temperature ( $T_m$ ) was calculated as the mid-log of the transition phase from the native to the denatured protein using a Boltzmann model in Protein Thermal Shift Software v1.3.  $\Delta T_m$  was calculated by subtracting reference melting temperature of proteins in the presence of H<sub>2</sub>O from the  $T_m$  in

the presence of heparin. Curve fitting was performed using the Boltzmann sigmoidal equation in Prism (v8) software.

### **Virus attachment assay**

Viral attachment assay was performed as previously described [58]. RD cells or Vero E6 cells at 80–90% confluency were precooled at 4 °C for 30 min, followed by infection with HCoV-OC43 (MOI of 40) or HCoV-NL63 (MOI of 30). After 2 h incubation at 4 °C, unbound viruses were removed by washing the cells two times with ice-cold PBS. The infected cells with viruses attached on cell surface were harvested for quantification by real-time qPCR or fixed for visualization by immunofluorescence staining.

### **RNA extraction and real-time PCR**

RNA extraction and RT-PCR were performed as previously described [59]. Total RNA was extracted using TRIzol reagents (Thermo Fisher Scientific). About 2.0 µg of total RNA was used to synthesize the first strand cDNA of viral RNA and host RNA using SuperScript III reverse transcriptase (Thermo Fisher Scientific) and Random Hexamer primers. After digestion of genomic DNA with RQ1 RNase-free DNase (Promega), target gene was amplified on a Thermal Fisher QuantStudio™ 5 Real-Time PCR System (Thermo Fisher Scientific) using FastStart Universal SYBR Green Master mix (carboxy-X-rhodamine; Roche) and following HCoV-NL63 N gene-specific primers (Forward: 5'-CTGTTACTTTGGCTTTAAAGAACT-TAGG-3'; Reverse: 5'-CTCACTATCAAAGAA-TAACGCAGCCTG-3') or HCoV-OC43 N gene-specific primers (Forward: 5'-CGATGAGGCTATTC CGACTAGGT-3'; Reverse: 5'- CCTTCCTGAGCCT TCAATATAGTAACC-3'). GAPDH was also amplified to serve as a control using human GAPDH-specific primers (GAPDH-F: 5'-ACACC-CACTCCTCCACCTTTG-3' and GAPDH-R: 5'-CACCACCCT GTTGCTGTAGCC-3'). The amplification conditions were: 95 °C for 10 min; 40 cycles of 15 s at 95 °C and 60 s at 60 °C. Melting curve analysis was performed to verify the specificity of each amplification. All experiments were repeated three times independently.

### **Molecular modelling of the binding of LF to HS**

Lactoferricin and dp4 were chosen as structural models for BLF and HSPGs, respectively. AutoDock Vina was used for modeling of binding of lactoferricin to dp4 [60]. Bovine lactoferricin (PDB: 1LFC) was set as the receptor and the docking grid box parameters were defined as the following: center\_x = 32.636,

center\_y = 76.438, center\_z = 46.275; size\_x = 106, size\_y = 120, size\_z = 104; exhaustiveness = 40. The heparin dp4 structure was downloaded from PDB code 5E9C. The final docking poses were generated in PyMOL. The protein electrostatics surface was generated using the APBS Electrostatics model in PyMOL.

### **Statistical analysis**

All experiments were performed in duplicates or triplicates. Data are shown as mean ± S.D. Statistical analysis was performed using GraphPad Prism Software 8.0 (GraphPad Software Inc., La Jolla, CA, USA). Comparisons were performed using two-tailed Student's *t*-test.

### **Combination therapy**

BLF was mixed with remdesivir at combination ratios of 8:1, 4:1, 2:1, 1:1, 1:2, 1:4, and 1:8, separately. The mixture of each compound with remdesivir at each combination ratio was serially diluted into 7 different concentrations and applied in HCoV-OC43 CPE assay to determine EC<sub>50</sub> of BLF and remdesivir in the combination ratio. CI<sub>s</sub> plot was used to depict the EC<sub>50</sub> values of each compound and remdesivir at different combination ratios. The red line indicates the additive effect, and above the red line indicates the antagonism, while below the red line indicates the synergy [39].

### **Acknowledgements**

SARS-Related Coronavirus 2, Isolate USA-WA1/2020 (NR-52281) was deposited by the Centers for Disease Control and Prevention and obtained through BEI Resources, NIAID, NIH.

### **Disclosure statement**

No potential conflict of interest was reported by the author(s).

### **Funding**

This research was partially supported by the National Institute of Allergy and Infectious Diseases of Health (NIH) (grants AI147325 and AI157046) and the Arizona Biomedical Research Commission Centre Young Investigator grant (ADHS18-198859) to J. W. Y.H. was supported by the NIH training grant T32 GM008804. The SARS-CoV-2 experiments were supported by a COVID-19 pilot grant from UTHSCSA and NIH grant AI151638 to Y.X.

### **ORCID**

Jun Wang  <http://orcid.org/0000-0002-4845-4621>

## References

- [1] Hui DS, Azhar EI, Madani TA, et al. The continuing 2019-nCoV epidemic threat of novel coronaviruses to global health – The latest 2019 novel coronavirus outbreak in Wuhan, China. *Int J Infect Dis.* 2020 Feb;91:264–266.
- [2] Gagneur A, Sizun J, Vallet S, et al. Coronavirus-related nosocomial viral respiratory infections in a neonatal and paediatric intensive care unit: a prospective study. *J Hosp Infect.* 2002 May;51(1):59–64.
- [3] Zumla A, Hui DS, Perlman S. Middle East respiratory syndrome. *Lancet.* 2015 Sep 5;386(9997):995–1007.
- [4] Mesel-Lemoine M, Millet J, Vidalain PO, et al. A human coronavirus responsible for the common cold massively kills dendritic cells but not monocytes. *J Virol.* 2012 Jul;86(14):7577–7587.
- [5] Vorland LH. Lactoferrin: a multifunctional glycoprotein. *APMIS.* 1999 Nov;107(11):971–981.
- [6] Wang Y, Wang P, Wang H, et al. Lactoferrin for the treatment of COVID-19 (Review). *Exp Ther Med.* 2020 Dec;20(6):272.
- [7] Kell DB, Heyden EL, Pretorius E. The biology of lactoferrin, an iron-binding protein that can help defend against viruses and bacteria. *Front Immunol.* 2020 May 28;11:1221.
- [8] Siqueiros-Cendon T, Arevalo-Gallegos S, Iglesias-Figueroa BF, et al. Immunomodulatory effects of lactoferrin. *Acta Pharmacol Sin.* 2014 May;35(5):557–566.
- [9] Russell-Jones G. Intestinal receptor targeting for peptide delivery: an expert's personal perspective on reasons for failure and new opportunities. *Ther Deliv.* 2011 Dec;2(12):1575–1593.
- [10] Kuwata H, Yamauchi K, Teraguchi S, et al. Functional fragments of ingested lactoferrin are resistant to proteolytic degradation in the gastrointestinal tract of adult rats. *J Nutr.* 2001 Aug;131(8):2121–2127.
- [11] Gajda-Morszewski P, Spiewak-Wojtyła K, Oszejca M, et al. Strategies for oral delivery of metal-saturated lactoferrin. *Curr Protein Pept Sci.* 2019;20(11):1046–1051.
- [12] Swart PJ, Kuipers ME, Smit C, et al. Antiviral effects of milk proteins: acylation results in polyanionic compounds with potent activity against human immunodeficiency virus types 1 and 2 in vitro. *AIDS Res Hum Retroviruses.* 1996 Jun 10;12(9):769–775.
- [13] Yi M, Kaneko S, Yu DY, et al. Hepatitis C virus envelope proteins bind lactoferrin. *J Virol.* 1997 Aug;71(8):5997–6002.
- [14] Pietrantoni A, Di Biase AM, Tinari A, et al. Bovine lactoferrin inhibits adenovirus infection by interacting with viral structural polypeptides. *Antimicrob Agents Chemother.* 2003 Aug;47(8):2688–2691.
- [15] Belting M. Heparan sulfate proteoglycan as a plasma membrane carrier. *Trends Biochem Sci.* 2003 Mar;28(3):145–151.
- [16] Waarts BL, Aneke OJ, Smit JM, et al. Antiviral activity of human lactoferrin: inhibition of alphavirus interaction with heparan sulfate. *Virology.* 2005 Mar 15;333(2):284–292.
- [17] Lang J, Yang N, Deng J, et al. Inhibition of SARS pseudovirus cell entry by lactoferrin binding to heparan sulfate proteoglycans. *PLoS One.* 2011;6(8):e23710.
- [18] Milewska A, Zarebski M, Nowak P, et al. Human coronavirus NL63 utilizes heparan sulfate proteoglycans for attachment to target cells. *J Virol.* 2014 Nov;88(22):13221–13230.
- [19] Naskalska A, Dabrowska A, Szczepanski A, et al. Membrane protein of human coronavirus NL63 is responsible for interaction with the adhesion receptor. *J Virol.* 2019 Oct 1;93(19):e00355–19.
- [20] Ahmed A, Siman-Tov G, Hall G, et al. Human antimicrobial peptides as therapeutics for viral infections. *Viruses.* 2019 Aug 1;11(8):704.
- [21] Tavassoly O, Safavi F, Tavassoly I. Heparin-binding peptides as novel therapies to stop SARS-CoV-2 cellular entry and infection. *Mol Pharmacol.* 2020 Nov;98(5):612–619.
- [22] Marr AK, Jenssen H, Moniri MR, et al. Bovine lactoferrin and lactoferricin interfere with intracellular trafficking of herpes simplex virus-1. *Biochimie.* 2009 Jan;91(1):160–164.
- [23] Clausen TM, Sandoval DR, Spliid CB, et al. SARS-CoV-2 infection depends on cellular heparan sulfate and ACE2. *Cell.* 2020 Nov 12;183(4):1043–1057.
- [24] Kim SY, Jin W, Sood A, et al. Characterization of heparin and severe acute respiratory syndrome-related coronavirus 2 (SARS-CoV-2) spike glycoprotein binding interactions. *Antiviral Res.* 2020 Sep;181:104873.
- [25] Yu J, Yuan X, Chen H, et al. Direct activation of the alternative complement pathway by SARS-CoV-2 spike proteins is blocked by factor D inhibition. *Blood.* 2020 Oct 29;136(18):2080–2089.
- [26] Zhang Q, Chen CZ, Swaroop M, et al. Heparan sulfate assists SARS-CoV-2 in cell entry and can be targeted by approved drugs in vitro. *Cell Discov.* 2020 Nov 4;6(1):80.
- [27] Crawford KHD, Eguia R, Dingens AS, et al. Protocol and reagents for pseudotyping lentiviral particles with SARS-CoV-2 spike protein for neutralization assays. *Viruses.* 2020 May 6;12(5):513.
- [28] Nie J, Li Q, Wu J, et al. Establishment and validation of a pseudovirus neutralization assay for SARS-CoV-2. *Emerg Microbes Infect.* 2020 Dec;9(1):680–686.
- [29] Hu Y, Ma C, Szeto T, et al. Boceprevir, calpain inhibitors II and XII, and GC-376 have broad-spectrum antiviral activity against coronaviruses in cell culture. *bioRxiv.* 2020 Nov 1. DOI:2020.10.30.362335
- [30] Hoffmann M, Kleine-Weber H, Schroeder S, et al. SARS-CoV-2 cell entry depends on ACE2 and TMPRSS2 and is blocked by a clinically proven protease inhibitor. *Cell.* 2020 Apr 16;181(2):271–280.
- [31] Shang J, Wan Y, Luo C, et al. Cell entry mechanisms of SARS-CoV-2. *Proc Natl Acad Sci USA.* 2020 May 26;117(21):11727–11734.
- [32] Tharappel AM, Samrat SK, Li Z, et al. Targeting crucial host factors of SARS-CoV-2. *ACS Infect Dis.* 2020 Nov 13;6(11):2844–2865.
- [33] Kong Q, Xiang Z, Wu Y, et al. Analysis of the susceptibility of lung cancer patients to SARS-CoV-2 infection. *Mol Cancer.* 2020 Apr 28;19(1):80.
- [34] Niesen FH, Berglund H, Vedadi M. The use of differential scanning fluorimetry to detect ligand interactions that promote protein stability. *Nat Protoc.* 2007;2(9):2212–2221.
- [35] Tree JA, Turnbull JE, Buttigieg KR, et al. Unfractionated heparin inhibits live wild type SARS-CoV-2 cell infectivity at therapeutically relevant concentrations. *Br J Pharmacol.* 2021 Feb;178(3):626–635.
- [36] Bayat Mokhtari R, Homayouni TS, Baluch N, et al. Combination therapy in combating cancer. *Oncotarget.* 2017 Jun 6;8(23):38022–38043.

- [37] van der Pluijm RW, Tripura R, Hoglund RM, et al. Triple artemisinin-based combination therapies versus artemisinin-based combination therapies for uncomplicated plasmodium falciparum malaria: a multicentre, open-label, randomised clinical trial. *Lancet*. 2020 Apr 25;395(10233):1345–1360.
- [38] De Clercq E, Li G. Approved antiviral drugs over the past 50 Years. *Clin Microbiol Rev*. 2016 Jul;29(3):695–747.
- [39] Ma C, Hu Y, Zhang J, et al. Pharmacological characterization of the mechanism of action of R523062, a promising antiviral for Enterovirus D68. *ACS Infect Dis*. 2020 Aug 14;6(8):2260–2270.
- [40] Shimazaki K, Tazume T, Uji K, et al. Properties of a heparin-binding peptide derived from bovine lactoferrin. *J Dairy Sci*. 1998 Nov;81(11):2841–2849.
- [41] Di Biase AM, Pietrantonio A, Tinari A, et al. Heparin-interacting sites of bovine lactoferrin are involved in anti-adenovirus activity. *J Med Virol*. 2003 Apr;69(4):495–502.
- [42] Drobni P, Naslund J, Evander M. Lactoferrin inhibits human papillomavirus binding and uptake in vitro. *Antiviral Res*. 2004 Oct;64(1):63–68.
- [43] Pietrantonio A, Ammendolia MG, Tinari A, et al. Bovine lactoferrin peptidic fragments involved in inhibition of echovirus 6 in vitro infection. *Antiviral Res*. 2006 Feb;69(2):98–106.
- [44] Andersen JH, Jenssen H, Sandvik K, et al. Anti-HSV activity of lactoferrin and lactoferricin is dependent on the presence of heparan sulphate at the cell surface. *J Med Virol*. 2004 Oct;74(2):262–271.
- [45] Andersen JH, Osbakk SA, Vorland LH, et al. Lactoferrin and cyclic lactoferricin inhibit the entry of human cytomegalovirus into human fibroblasts. *Antiviral Res*. 2001 Aug;51(2):141–149.
- [46] Hwang PM, Zhou N, Shan X, et al. Three-dimensional solution structure of lactoferricin B, an antimicrobial peptide derived from bovine lactoferrin. *Biochemistry*. 1998 Mar 24;37(12):4288–4298.
- [47] Wu L, Viola CM, Brzozowski AM, et al. Structural characterization of human heparanase reveals insights into substrate recognition. *Nat Struct Mol Biol*. 2015 Dec;22(12):1016–1022.
- [48] Tree JA, Turnbull JE, Buttigieg KR, et al. Unfractionated heparin inhibits live wild type SARS-CoV-2 cell infectivity at therapeutically relevant concentrations. *Br J Pharmacol*. 2021 Feb;178(3):626–635.
- [49] Milewska A, Nowak P, Owczarek K, et al. Entry of human coronavirus NL63 into the cell. *J Virol*. 2018 Jan 17;92(3):e01933–17.
- [50] Mirabelli C, Wotring JW, Zhang CJ, et al. Morphological cell profiling of SARS-CoV-2 infection identifies drug repurposing candidates for COVID-19. *bioRxiv*. 2020 Jun 10. DOI:2020.05.27.117184.
- [51] de Carvalho CAM, da Rocha Matos A, Caetano BC, et al. In vitro inhibition of SARS-CoV-2 infection by bovine lactoferrin. *bioRxiv*. 2020. DOI:2020.05.13.093781.
- [52] Hu Y, Zhang J, Musharrafieh RG, et al. Discovery of dapivirine, a nonnucleoside HIV-1 reverse transcriptase inhibitor, as a broad-spectrum antiviral against both influenza A and B viruses. *Antiviral Res*. 2017 Sep;145:103–113.
- [53] Ma C, Sacco MD, Hurst B, et al. Boceprevir, GC-376, and calpain inhibitors II, XII inhibit SARS-CoV-2 viral replication by targeting the viral main protease. *Cell Res*. 2020 Aug;30(8):678–692.
- [54] Zhang J, Hu Y, Wu N, et al. Discovery of influenza polymerase PA-PB1 interaction inhibitors using an in vitro split-luciferase complementation-based assay. *ACS Chem Biol*. 2020 Jan 17;15(1):74–82.
- [55] Ma C, Li F, Musharrafieh RG, et al. Discovery of cyclosporine A and its analogs as broad-spectrum anti-influenza drugs with a high in vitro genetic barrier of drug resistance. *Antiviral Res*. 2016 Sep;133:62–72.
- [56] Zhang J, Hu Y, Hau R, et al. Identification of NMS-873, an allosteric and specific p97 inhibitor, as a broad antiviral against both influenza A and B viruses. *Eur J Pharm Sci*. 2019 May 15;133:86–94.
- [57] Musharrafieh R, Ma C, Zhang J, et al. Validating Enterovirus D68-2A(pro) as an antiviral drug target and the discovery of Telaprevir as a potent D68-2A (pro) inhibitor. *J Virol*. 2019 Mar 21; 93(7):e02221–18.
- [58] Ma C, Hu Y, Zhang J, et al. A novel capsid binding inhibitor displays potent antiviral activity against Enterovirus D68. *ACS Infect Dis*. 2019 Nov 8;5(11):1952–1962.
- [59] Zhang J, Hu Y, Foley C, et al. Exploring Ugi-Azide four-component reaction products for broad-spectrum influenza antivirals with a high genetic barrier to drug resistance. *Sci Rep*. 2018 Mar 15;8(1):4653.
- [60] Trott O, Olson AJ. Autodock Vina: improving the speed and accuracy of docking with a new scoring function, efficient optimization, and multithreading. *J Comput Chem*. 2010 Jan 30;31(2):455–461.